Supporting Information

Title: Electrochemical and electromechanical properties of superior-performance hybrid polymer actuators exhibiting synergistic effects due to manganese oxide and multiwalled carbon nanotubes on various ionic liquids

Authors: Naohiro Terasawa*, Kinji Asaka

Affiliation:

Inorganic Functional Material Research Institute, National Institute of Advanced Industrial Science and Technology (AIST), 1-8-31 Midorigaoka, Ikeda, Osaka 563-8577, Japan

Tel: +81-72-751-7914, Fax: +81-72-751-8370

E-mail: terasawa-naohiro@aist.go.jp

a)

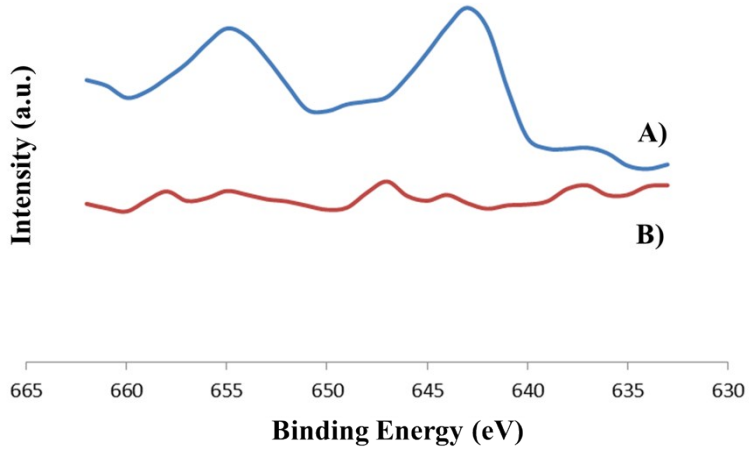
Intensity (a.u.)
A)
B)
665
660
655
650
645
640
635
630
Binding Energy (eV)

b)

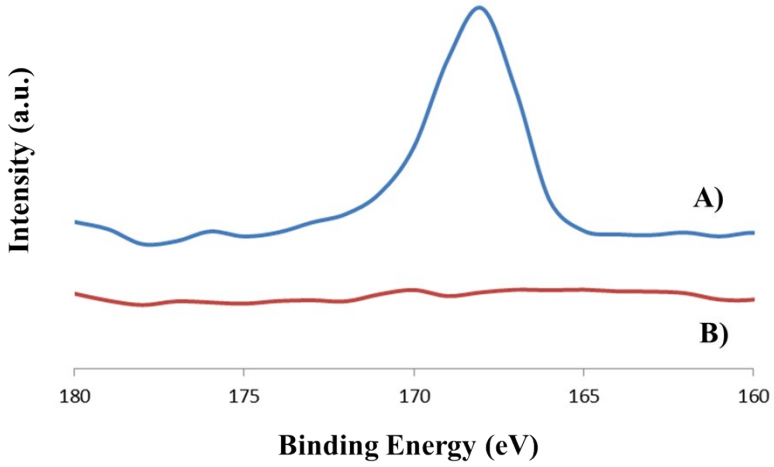
Intensity (a.u.)
A)
B)
180
175
170
165
160
Binding Energy (eV)

c)

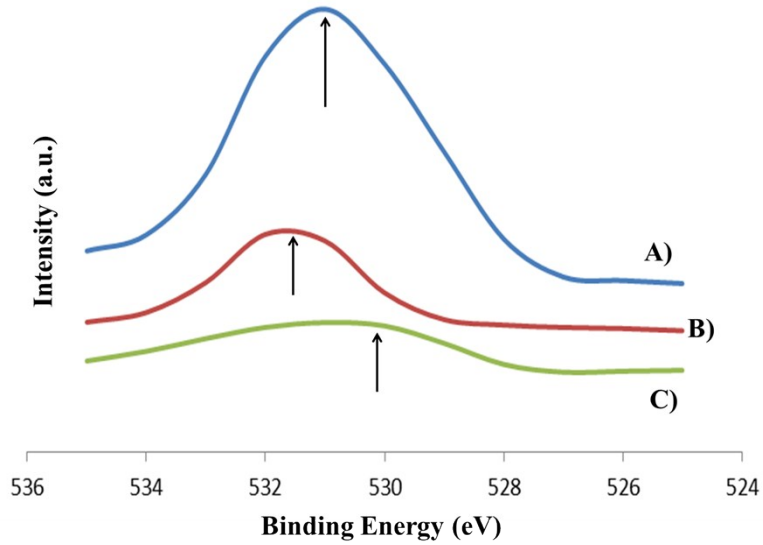

Fig. S1 Comparison of XPS results for various polymer-supported MWCNT/IL gel electrode layers containing MnO_2: a) Mn_{2p} region: MnO_2/MWCNT/EMI[BF_4]/PVdF(HFP) (MnO_2:MWCNT = 1:1, blue line) and (MnO_2:MWCNT = 0:1, red line); b) S_{2p} region: MnO_2/MWCNT/EMI[CF_3SO_3]/PVdF(HFP) (blue line) (MnO_2:MWCNT = 1:1) and MnO_2/MWCNT/EMI[BF_4]/PVdF(HFP) (red line) (MnO_2:MWCNT = 1:1); and c) O_{1s} region: MnO_2/MWCNT/EMI[CF_3SO_3]/PVdF(HFP) (MnO_2:MWCNT = 1:1, blue line) and (MnO_2:MWCNT = 0:1, red line), and MnO_2/MWCNT/EMI[BF_4]/PVdF(HFP) (MnO_2:MWCNT = 1:1, green line).

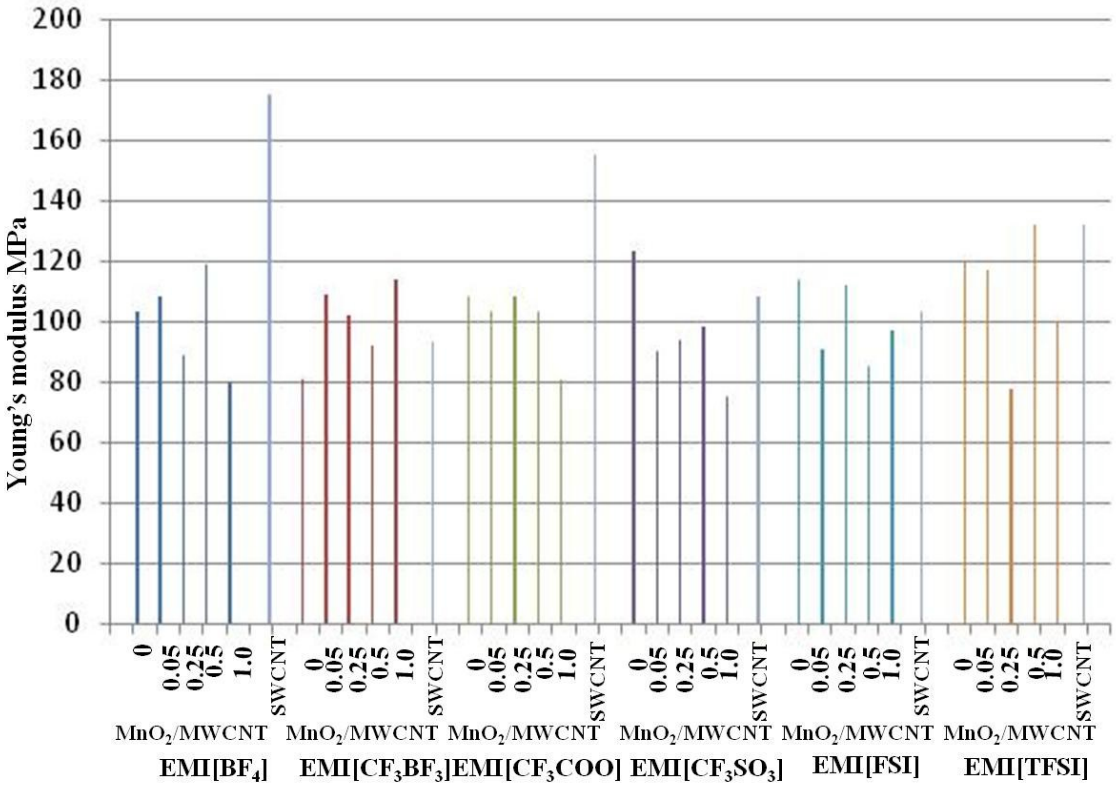

Fig. S2 Comparison of Young's moduli for various polymer-supported MWCNT/IL gel electrode layers containing MnO_2.

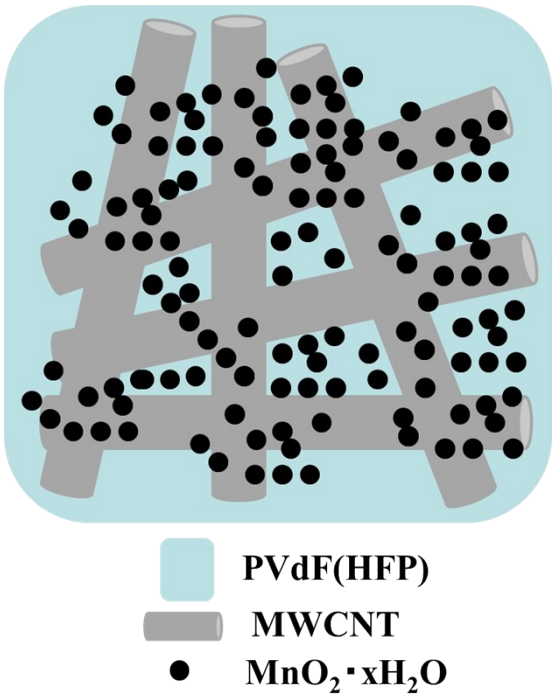

Fig. S3 Schematic of highly entangled MWCNTs forming a network of open mesopores, allowing the easy access of ions to the bulk of the MnO_2.

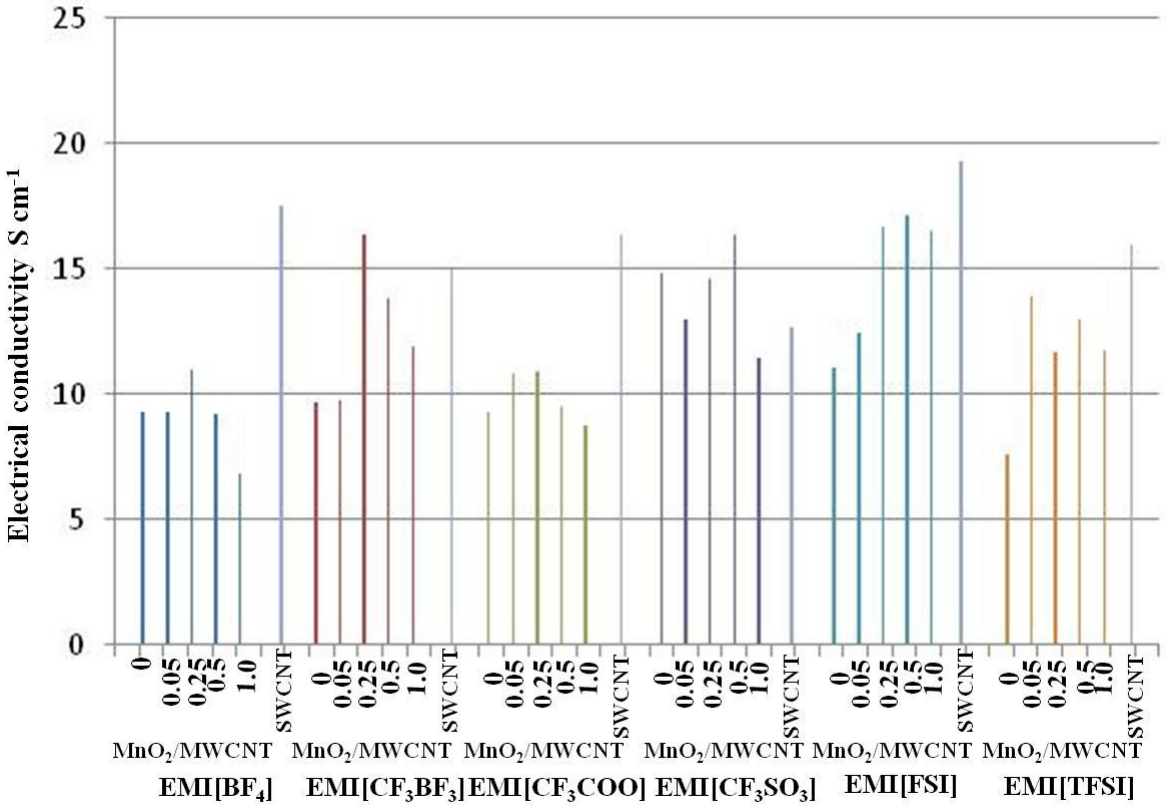

Fig. S4 Comparison of the electrical conductivities of various polymer-supported MWCNT/IL gel electrode layers containing MnO_2.

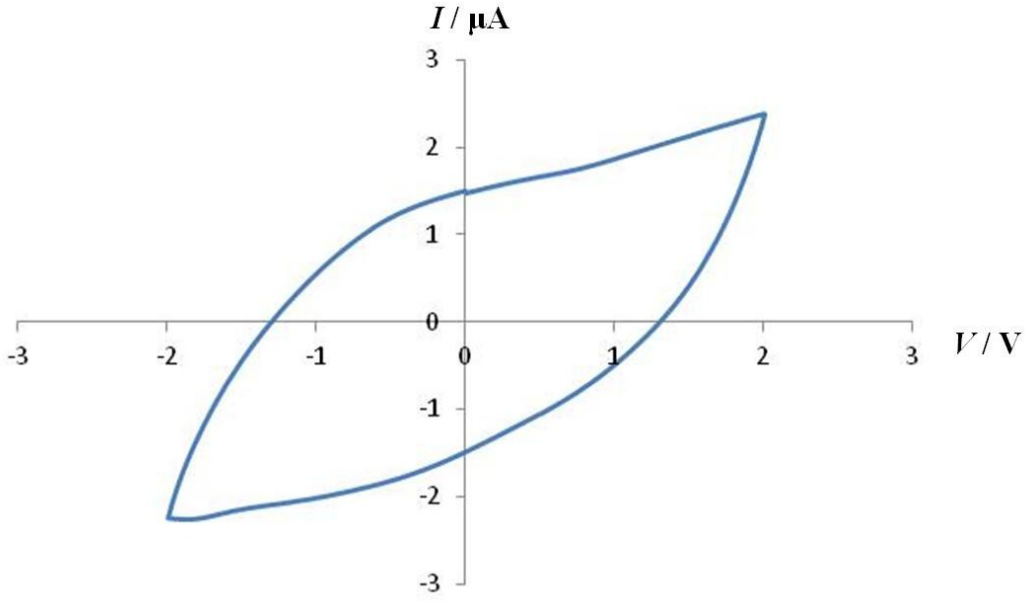

Fig. S5 CV of a cell system composed of an IL (EMI[CF_3BF_3]) electrolyte sandwiched between two non-MWCNT gel electrode layers ($MnO_2 \cdot xH_2O$/EMI[CF_3BF_3]/PVdF(HFP) = 5:12:8) (applied triangular voltage: ±2.0 V, sweep rate = 40 mV s^{-1} (0.005 Hz)).

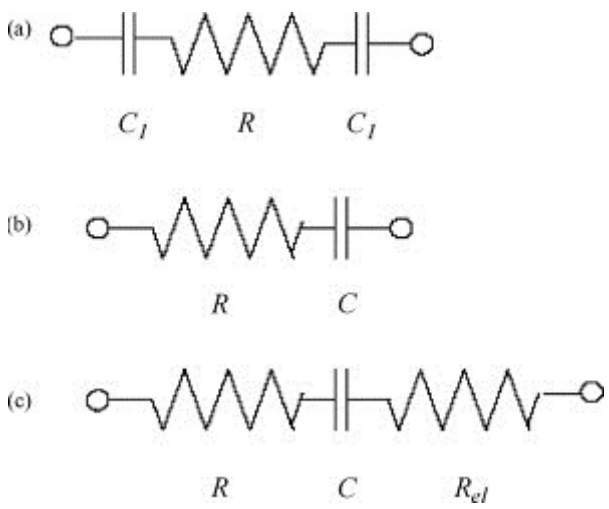

Fig. S6 Equivalent circuit model of a bucky-gel actuator. (a) A model composed of the double-layer capacitance, C_1, and ionic resistance, R; (b) a model in which the double-layer capacitance is represented by $C = C_1/2$; and (c) a model composed of C, R, and the electrode resistance, R_{el}.

Table S1 Simulation parameter values.

IL	C_{MWCNT} (F g^{-1})	C (F cm^{-2})	κ (mS cm^{-1}) [a)]	R (Ω cm^2)	ε_0 (%)	CR (s)
EMI[BF_4]	**196.37**	**0.0966**	**2.8**	**0.714**	**1.67**	**0.0691**
EMI[CF_3BF_3]	**106.84**	**0.0633**	**2.8**	**0.716**	**0.99**	**0.0453**
EMI[CF_3COO]	**135.08**	**0.0702**	**1.6**	**1.251**	**1.85**	**0.0878**
EMI[CF_3SO_3]	**144.97**	**0.0519**	**4.4**	**0.455**	**1.35**	**0.0236**
EMI[FSI]	**111.59**	**0.0658**	**4.5**	**0.444**	**0.84**	**0.0292**
EMI[TFSI]	**106.8**	**0.0636**	**1.2**	**1.669**	**1.23**	**0.1061**

[a)] ref. [10]

Table S2 Simulation parameter values with consideration of the electrode resistance.

IL	C (F cm^{-2})	R_{el}(Ω cm^2)	$R+R_{el}$ (Ω cm^2)	$C(R+R_{el})$ (s)
EMI[BF_4]	**0.0966**	**11.4**	**12.11**	**1.17**
EMI[CF_3BF_3]	**0.0633**	**19.9**	**20.62**	**1.305**
EMI[CF_3COO]	**0.0702**	**13.6**	**14.85**	**1.043**
EMI[CF_3SO_3]	**0.0519**	**19.1**	**19.56**	**1.015**
EMI[FSI]	**0.0658**	**27.6**	**28.04**	**1.845**
EMI[TFSI]	**0.0636**	**19.6**	**21.27**	**1.353**

R_{el} = area of the electrode film (**cm^2**)/(electrical conductivity (**S cm^{-1}**) × thickness of the electrode film (**cm**)) **(Ref. (6))**

Figure S6 shows the equivalent circuit models for the MnO_2•xH_2O/MWCNT polymer actuators. The model shown in Figure S6(a) consists of the specific capacitance, C_1, between the MnO_2•xH_2O/MWCNT electrode and the electrolyte layer; and the resistance, R, associated with the electrolyte layer. Figure S6(b) shows a more simplified model, in which the two C_1 capacitances are replaced by a single capacitance, C (= C_1/2). When a triangular voltage with amplitude ±A and frequency f is applied to the equivalent circuit shown in Figure S6(b), the maximum accumulated charge, $Q(f)$, can be expressed as shown in Eq. S1.[S1]

$$Q(f)/Q_0 = 1 - 4CRf\,(1 - \exp(-1/4CRf)) \quad \text{(S1)}$$

where Q_0 is the accumulated charge at the low-frequency limit.

If the strain, ε, in the electrode layer is proportional to the accumulated charge, it can be calculated according to Eq. S2.

$$\varepsilon = \varepsilon_0 \, Q(f) / Q_0, \tag{S2}$$

where ε_0 is the strain at the low-frequency limit.

When considering conduction in the electrode layer, the electrode resistance must be accounted for in the equivalent circuit. If the electrode resistance is treated explicitly, the equivalent circuit should be treated as a distributed transmission line.[S2] Here, we assume that the electrode resistance consists of a resistance element, R_{el}, as shown in Figure S6(c), so that R in Eq. S1 can be replaced by $R + R_{el}$.

To evaluate the double-layer charging kinetic model (which accounts for the oxidization and reduction reactions for metal oxides), the specific capacitance of the MnO_2•xH_2O/MWCNT electrode and the ionic resistance of the gel electrolyte layer were measured. The frequency dependence of the strain was calculated using Eqs. S1 and S2. Figure S7 shows the frequency dependence of the measured strain values, together with the simulation results for the MnO_2•xH_2O/MWCNT/EMI[BF_4] device. Curve A was calculated using the model shown in Figure S6(b); Table S1 lists the simulation parameters. Curve B was calculated using the model shown in Figure S6(c). The corresponding simulation parameters are listed in Table S2. It is clear from Figure S7 that the frequency dependence of the strain is well reproduced by Curve B. Further, it is clear from Figure S7 that the frequency dependence of the strain is reproduced by the double-layer charging kinetic model when one

considers the electrode resistance. Similar results were obtained for the MnO_2•xH_2O/MWCNT/IL devices based on other ILs. To fit the strain values in the low-frequency limit shown in Figure S6, appropriate values were chosen for ε_0 in Eq. S2. These are listed in Table S2.

To optimize the performance of the actuator, the results summarized in Tables S1 and S2 should be considered with respect to both the kinetic and static components. From a kinetic viewpoint, the frequency dependence of the strain is determined by electrochemical charging, as shown in Figure S7. Generally, to obtain good fits, the electrode resistance must be taken into consideration. The responses of the MnO_2•xH_2O/MWCNT polymer actuators can be improved by fabricating electrodes with higher conductivities.

The time constant is represented by the equivalent circuit in a series combination of the ionic resistance, R; double-layer capacitance, C; and electrode resistance, R_{el}. With regard to kinetics, Eqs. S1 and S2 show that strain is related to the time constant. The simulated results (solid curve B in Fig. S7) indicate the strain dependence on the frequency for the MnO_2/MWCNT (MnO_2:MWCNT = 1.0) gel actuator containing various ILs (Fig. 9). In the case of MnO_2 at high frequencies (0.1–10 Hz), since the time constant ($C(R+R_{el})$) shows the trend EMI[CF_3SO_3] ≒ EMI[CF_3COO] ≒ EMI[BF_4] > EMI[CF_3BF_3] ≒ EMI[TFSI] > EMI[FSI], the actuator strain trend is EMI[CF_3SO_3] ≒ EMI[CF_3COO] ≒ EMI[BF_4] < EMI[CF_3BF_3] ≒ EMI[TFSI] < EMI[FSI].

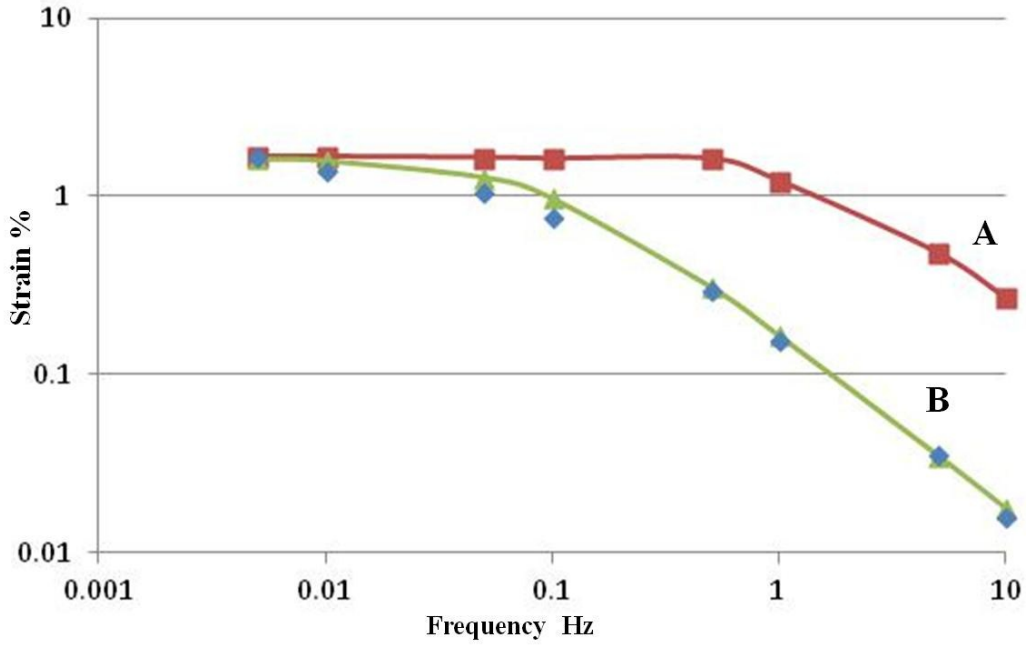

Fig. S7 Measured (blue symbols) and simulated results (Curves A and B) showing the frequency dependence of the strain for the MnO_2•xH_2O/MWCNT/EMI[BF_4] device. Curve A was calculated using the equivalent circuit shown in Figure S6(b). Curve B was calculated using the equivalent circuit shown in Figure S6(c).

Reference

[S1] I. Takeuchi, K. Asaka, K. Kiyohara, T. Sugino, K. Mukai, T. Fukushima and T. Aida, *Electrochim. Acta*, 2009, **53**, 1762–1768.

[S2] K. Takagi, Y. Nakabo, Z-W Luo and K. Asaka, *Proceedings of the SPIE, Electroactive Polymer Actuator and Devices (EAPAD),* 2007, **6524**, 652416-1–8.